Characterization and Diagnostics of Active Phased Array Modules Using Non-Invasive Electro-Optic Field Probes with a CW Laser Source

Kazem Sabet[1], Richard Darragh[1], Ali Sabet[1], Kamal Sarabandi[2], Khalid Jamil[3], and Sami Alhumaidi[3]
[1]EMAG Technologies, Ann Arbor, MI 48108 USA
[1]The University of Michigan, Ann Arbor, MI 48109 USA
[2]King Saud University, Riyadh, Saudi Arabia

***Abstract*—Electro-optic (EO) field probes can be used very effectively for simultaneous near-field and far-field characterization of radiating apertures. Due to their very small footprint and absence of any metallic parts at the signal pickup area, EO probes provide a non-invasive method for ultra-wideband measurement of aperture-level fields in RF circuits and antennas with very high spatial resolution. In this paper, we describe the use of EO field probes with a CW laser source to characterize a vertically integrated X-band active phased array tile and verify the measured results with simulation data and anechoic chamber measurements.**

***Index Terms*—Active phased array, radiation pattern, near-field scanning, electro-optic field probe.**

I. Introduction

The recent advances in the state of the art of monolithic microwave integrated circuit (MMIC) technology have inspired innovative packaging schemes for active electronically scanned array (AESA) antennas. AESA architectures integrate radiating elements and frequency conversion and amplification stages along with digital beamforming networks or other beam shaping/steering devices such as phase shifters and attenuators. During the last two decades, different types of AESA architectures have been proposed including wafer-scale system-on-chip concepts [1] and those based on printed circuit board (PCB) manufacturing processes [2]. Active phased array modules are typically characterized using port-based measurements with a vector network analyzer. The radiation patterns of active phased arrays are typically measured in an anechoic chamber. Near-field scanning systems provide a compact alternative to anechoic chambers based on the near-to-far-field transformation theory. Conventional near-field scanning systems use one or more metallic radiators or probes to sample the fields of the device under test (DUT). Such probes, however, cannot get very close to the DUT because the presence of an intruding external metallic structure inadvertently perturbs the fields of the DUT. As a result, the spatial resolution of these systems is often poor, and they cannot be used effectively for diagnostic purposes.

The use of electro-optic field probes for near-field mapping of RF devices and antennas has been explored in the past [3]-[5]. The previous work utilized the optical beam from a phase-stabilized ultrafast pulsed laser system with an optical wavelength of 900nm and a pulse output of 100fs duration at an 80MHz pulse repetition rate. The RF signal supplied to the DUT by the microwave synthesizer was synchronized to the laser pulse train using the phase-locked-loop electronics of the stabilized laser system. The electrical signal from the output of the photodetector was measured in a harmonic mixing scheme at an intermediate frequency (IF) that was derived from the difference between the input signal frequency and an integer harmonic of the 80MHz repetition rate.

A far more streamlined EO field probe system has recently been developed based on a commercial 1550nm continuous wave (CW) laser diode source [6]. The new EO probe and the associated optical processing mainframe utilize polarization maintaining (PM) fiber throughout the optical chain to achieve a high degree of polarization stability; hence, better sensitivity and repeatability. Since the new EO probe system does not require synchronization with a laser pulse train, it provides a superior and more stable phase measurement capability. Accurate and reproducible phase measurement is particularly critical for the application of the near-to-field transformation required for the computation of far-field radiation patterns. In this paper, we present the measurement results from EO mapping of a vertically integrated 16-channel X-band AESA tile and verify them using both simulation data and measurement data collected in an anechoic chamber. We will show how the near-field maps can be used for pattern characterization of the AESA at different beam steer angles as well as for the diagnostics of malfunctioning channels.

II. Vertically Integrated X-Band AESA Module

In the vertically integrated packaging architecture considered in this paper, an AESA tile is made up of several interconnected stacked layers. The topmost layer stack contains the radiating elements and their feed network infrastructure. In the X-band AESA tile shown in Fig. 1, the radiators are microstrip-fed slot-coupled patch antennas printed on a 1.5mm-thick Roger RO 4003C substrate.

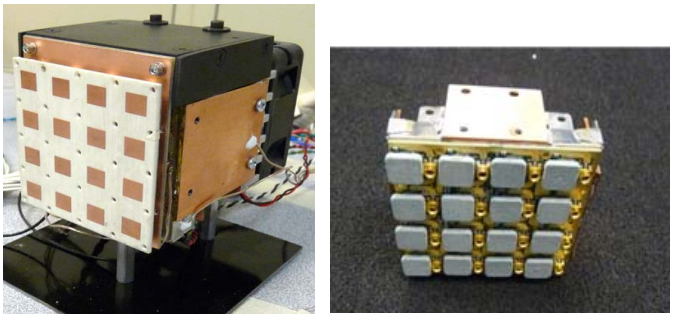

Fig. 1. Pictures of the 16-element X-band AESA module: (Left) a complete tile with integrated thermal management system and rear fan, (Right) the frequency conversion board showing 16 active up-converters and 16 SMPM connectors feeding the upper antenna board.

978-1-5090-6360-4/17/$31.00 ©2017 IEEE

The microstrip feed lines are printed on a 0.2mm-thick substrate of the same material. Each tile contains a total of 16 patch antennas arranged in a 4×4 rectangular grid with a uniform spacing of 15mm. The total area of the tile aperture is 60mm×60mm. The next layer stack in the hierarchy contains 16 active frequency up-converters together with 16 quadrature hybrid couplers. Also included in this stack is a 1:16 signal distribution network for the local oscillator at 8GHz, which is generated by a phase-locked loop (PLL) frequency synthesizer. The third layer stack is responsible for beam shaping and steering. It contains 16 digital phase shifter and 16 digital attenuators. The fourth layer stack at the bottom of the tile contains a 16-bit integrated microcontroller/digital signal processor that commands and controls all the digital devices using a serial peripheral interface (SPI) bus. The AESA tiles can be daisy-chained to achieve scalable larger apertures. The AESA transmitter tile of Fig. 1 produces an effective isotropic radiated power (EIRP) of 14-15dBW at 9.5GHz with a bandwidth of 500MHz.

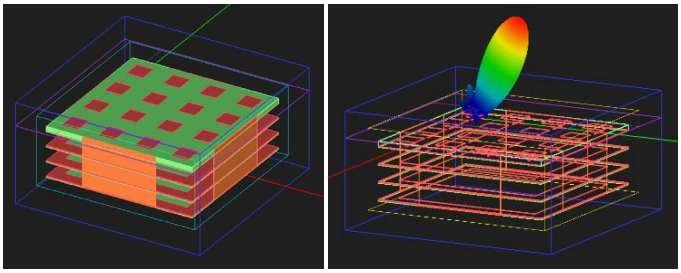

Fig. 2. The simulation setup for the FDTD analysis of the AESA tile. The lateral copper plates are part of the integrated thermal management system.

In order to verify the measurement results using the EO field probes, the AESA tile was simulated using EM.Cube's finite difference time domain (FDTD) solver (www.emagtech.com). Fig. 2 above shows the geometry of the AESA tile's stacked layer hierarchy with the antenna board at the top and three additional layer stacks underneath it. The feed lines on the bottom side of the antenna board are excited using 16 microstrip ports with individual excitation waveforms including user defined amplitudes and phases. Fig. 2 shows the simulated 3D radiation pattern of the AESA tile with a beam steering of $\theta = 30°$ and $\phi = 90°$ in the principal YZ plane at 9.5GHz. For the sake of simplicity, the lower layer stacks are assumed to contain two dielectric layers with a sandwiched metal ground plane in between.

III. Electro-Optic Field Probes

An electro-optic field probe consists of an electro-optic (EO) crystal cut along one of its optical axes and mounted at the tip of an optical fiber via a graded index (GRIN) lens as shown in Fig. 3. The CW laser beam propagating through the optical fiber and then into the EO crystal experiences the Pockels effect, whereby its polarization vector is rotated due to the presence of an impinging radio frequency (RF) electric field [6]. The change in the polarization state of the optical beam is linearly proportional to the amplitude of the electric field generated by the DUT. Since the EO crystals are anisotropic, the three field components along the X, Y and Z directions can be measured with a high level of polarization discrimination. The phase of the input signal exciting the DUT is synchronized with the phase of the RF data acquisition system at the output of the photodetector using a lock-in amplifier. The system shown in Fig. 3 can measure both amplitude and phase of the three electric field components simultaneously with very high repeatability.

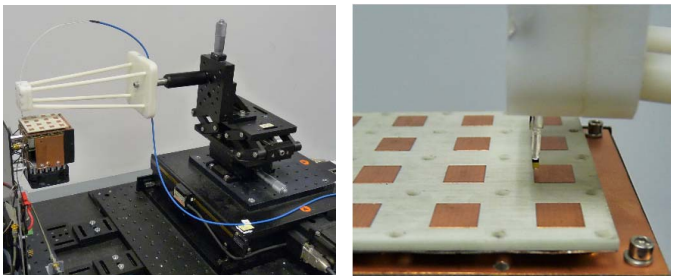

Fig. 3. Pictures of the CW-EO field measurement system with a PM-fiber-based electro-optic field probe mounted on a plastic holder fixture attached to a computer-controlled precision X-Y translation stage.

IV. EO Near-Field Scanning of the AESA Tile

The CW-EO near-field mapping system was set up to map the aperture field of the X-band AESA tile with a total scan area of 70mm×70mm as shown in Fig. 3. Two sets of measurements were carried out: one at a probe height of 0.6mm above the array tile with a finer scan step of 0.5mm (140×140 points), and the other at a probe height of 1.5mm with a lower-resolution scan step of 1mm (70×70 points). Fig. 4 compares the measured and simulated data for the electric field distribution at a height of 0.6mm. Next, the 16 digital phase shifters were given a phase progression of -90° to steer the array's beam elevation by 30° from the zenith in the YZ-plane. Fig. 5 compares the measured and simulated phase data for the tangential electric field components at a height of 1.5mm above the array tile.

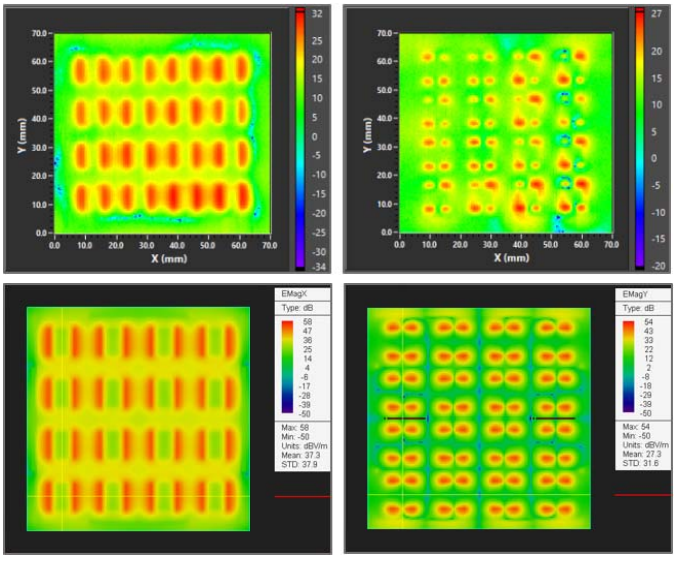

Fig. 4. A comparison of measured (Top) and simulated (Bottom) near-field maps of the AESA tile at a height of 0.6mm above the aperture: (Left) amplitude of Ex component, and (Right) amplitude of Ey component.

978-1-5090-6360-4/17/$31.00 ©2017 IEEE

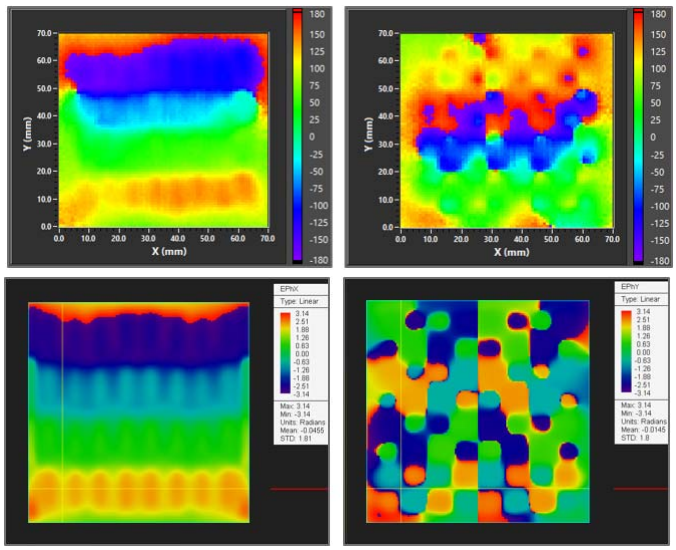

Fig. 5. A comparison of measured (Top) and simulated (Bottom) near-field phase maps of the AESA tile with a beam steering of $\theta = 30°$ and $\phi = 30°$ at a height of 1.5mm above the aperture: (Left) phase of Ex component, and (Right) phase of Ey component.

The measured amplitude and phase field maps were used to compute that far-field radiation patterns of the tile using the near-to-field transformation. The results are shown in Fig. 6 and compared to simulation results as well as measured results using a conventional anechoic chamber for the two cases of no beam steering ($\theta = \phi = 0°$) and a beam steering of $\theta = 30°$ and $\phi = 90°$. A good agreement is observed among all the data sets.

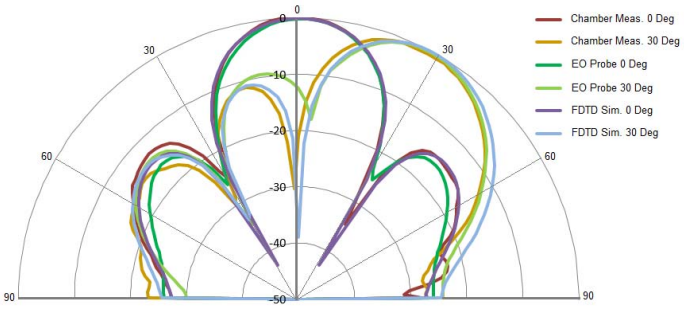

Fig. 6. A comparison of measured and simulated far-field radiation patterns of the AESA tile with no beam steering ($\theta = \phi = 0°$) and a beam steering of $\theta = 30°$ and $\phi = 30°$. The graph shows two sets of measured data, one using the EO probe and another collected in an anechoic chamber.

V. Using EO Near-Field Maps for Array Diagnostics

The multilayer boards of the AESA tile are interconnected using miniaturized SMPM connectors. These connectors use small bullets to provide good mechanical maneuverability. As the next step, we removed one of these bullets to disconnect the patch element (3, 3) from its power amplifier in the lower board. In the FDTD simulation, a zero amplitude weight was assigned to the excitation source of this element. Fig. 7 shows and compares the measured and simulated amplitude and phase maps of the E_x field component. Note that the location of the malfunctioning power amplifier stands out visibly in both amplitude and phase maps.

VI. Conclusion

It was demonstrated that non-invasive EO field probes can generate "true" near-field maps of AESA modules for diagnostic purposes. The same set of measurement data can be used to produce accurate far-field radiation patterns at different beam steering angles due to the superior phase measurement capability of the new PM-fiber-based CW-EO field mapping system.

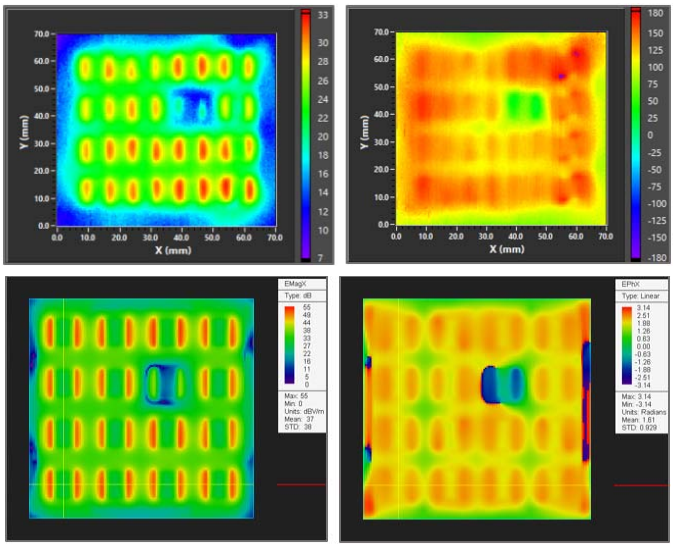

Fig. 7. A comparison of measured (Top) and simulated (Bottom) near-field maps of the AESA tile with a missing connector bullet: (Left) amplitude of Ex component, and (Right) phase of Ex component.

References

[1] D. Shin, C-Y Kim, D-W Kang and Gabriel M. Rebeiz, "A high-power packaged four-element X-band phased-array transmitter in 0.13-μ CMOS for radar and communication systems," *IEEE Trans. Microw. Theory Tech.,* vol. 61, no. 8, pp. 3060-3071, Aug. 2013.

[2] C.E. Patterson, T.K. Thrivikraman, A.M. Yepes, S.M. Begley, S. K. Bhattacharya, J.D. Cressler and John Papapolymerou, "A lightweight organic X-band active receiving phased array with integrated SiGe amplifiers and phase shifters," *IEEE Trans. Antennas Propagat..,* vol. 59, no. 1, pp. 100-109, Jan. 2011.

[3] K. Yang, G. David, J-G Yook, I. Papapolymerou, L.P. B. Katehi and J.F. Whitaker, "Electrooptic mapping and finite-element modeling of the near-field pattern of a microstrip patch antenna," *IEEE Trans. Microw. Theory Tech.,* vol. 48, no. 2, pp. 288-294, Feb. 2000.

[4] K. Yang, T. Marshall, M.l Forman, J. Hubert, L. Mirth, Z. Popovic, L.P. B. Katehi and J.F. Whitaker, "Active-amplifier-array diagnostics using high-resolution electrooptic field mapping," *IEEE Trans. Microw. Theory Tech.,* vol. 49, no. 5, pp. 849-857, May 2001.

[5] R.M. Reano, K. Yang, L.P. B. Katehi and J.F. Whitaker, "Simultaneous measurements of electric and thermal fields utilizing an electrooptic semiconductor probe," *IEEE Trans. Microw. Theory Tech.,* vol. 49, no. 12, pp. 2523 -2531, Dec. 2001.

[6] K. Sabet, R. Darragh, A. Sabet and S. Hatch, "Characterization of dual-band circularly polarized active electronically scanned arrays (AESA) using electro-optic field probes," *presented at* the *38th Annual Meeting and Symposium of the Antenna Measurement Techniques Association (AMTA),* Austin, TX, Oct. 30 - Nov. 4, 2016.

978-1-5090-6360-4/17/$31.00 ©2017 IEEE